https://doi.org/10.5194/gmd-2019-298
Preprint. Discussion started: 24 February 2020

Geoscientific Model Development
Discussions
Open Access

Intercomparison between the Integrated Urban land Model and the Noah Urban Canopy Model

Chunlei MENG Junxia DOU

Institute of Urban Meteorology, China Meteorological Administration, 100089, Beijing, China.

Corresponding author: Dr. Chunlei Meng, Institute of Urban Meteorology, China Meteorological Administration, Beijing, 100089, China. No.55 Beiwaxili, Haidian District, Beijing, China. E-mail: clmeng@ium.cn
Mobile:(86)13811346500

https://doi.org/10.5194/gmd-2019-298
Preprint. Discussion started: 24 February 2020

Geoscientific Model Development Discussions
Open Access

Abstract

Urban land surface model (ULSM) is an important tool to study the climatic effect of human activity. Now there are two main methods to parameterize the effects of human activity, the coupling method and the integrating method. For the coupled method, the urban canopy model (UCM) was developed and coupled with the land surface model for the natural land surfaces. For the integrated method, the urban land surface model was built directly based on the traditional land surface model. In this paper, the Noah Single Layer Urban Canopy Model (Noah/SLUCM) and the Integrated Urban land Model (IUM) were compared using the observed fluxes data at the 325-meter meteorology tower in Beijing. Through the comparison, the key factors and physical processes of the urban land surface model which have significant impact on the performance of ULSM were found out. The results indicate that the absorbed solar radiation of urban surface was reduced by the solar radiation scattering, the absorption of building roof and wall, and the shading effect of urban canopy and tall buildings. Urban surface roughness length and friction velocity are important in urban sensible heat flux simulation. Urban water balance and impervious surface evaporation (ISE) are important in urban latent heat flux simulation.

Key words: integrated urban land model; urban canopy model; reduction coefficient of solar absorption; impervious surface evaporation; urban water balance

https://doi.org/10.5194/gmd-2019-298
Preprint. Discussion started: 24 February 2020

Geoscientific Model Development Discussions
Open Access

1. Introduction

China now is experiencing an unprecedented urbanization movement. The regional climate could be changed by urbanization through the greenhouse gases emission, land use and land cover change (LUCC), and anthropogenic heat release (AHR) (Committee on Urban Meteorology 2012). The impact of land use and land cover change (LUCC) on climate change has the same order of magnitude as the impact of greenhouse gases emissions (Kalnay and Cai 2003; Sun et al. 2016). Urban land surface model is an important tool to study the climatic effect of urbanization. Now there are two main methods to parameterize the effects of human activity. One is the coupled method and the other is the bulk or integrated method. For the coupled method, the urban canopy model (UCM) (e.g. Kusaka et al. 2001; Kusaka and Kimura 2004) was developed and coupled with the land surface model for the natural land surfaces. For the integrated method (e.g. Meng 2015), the urban land surface model was built directly based on the traditional land surface model.

Model intercomparison is an effective method to evaluate different land surface models. Through the comparison, the key factors of the urban land surface model were found out. In the 1990s, the Project for Intercomparison of Land Surface Parameterization Schemes (PILPS) (Henderson-Sellers and Brown 1992; Henderson-Sellers et al. 1993, 1995) was launched to compare land surface models. Along the development of the urban land surface parameterization schemes, urban land surface model comparison project (Grimmond et al. 2010, 2011; Best and Grimmond 2015) was launched. The results indicate that the urban database (Ching et al. 2009; Demuzere et al. 2017; Hammerberg et al. 2018; He et al. 2015; Loridan and Grimmond 2012) is very important to urban land surface models. Compared with

https://doi.org/10.5194/gmd-2019-298
Preprint. Discussion started: 24 February 2020

Geoscientific Model Development Discussions

the parameterization of the urban energy balance processes, recently developed urban land surface models could not parameterize the urban water balance (Grimmond et al. 1986; Mitchell et al. 2001; Wang et al. 2013; Miao and Chen 2014; Yang et al. 2015) processes accurately. Albedo and fractional vegetation cover are important parameters in urban land surface model, while the AHR is only important in certain cities.

However, these intercomparison studies only concern the impact of the bulk model and UCM with different complexity on surface radiation and energy balances. In this paper, different from the models used for intercomparison in Best and Grimmond (2015), the Integrated Urban land Model (IUM) (Meng 2015) was introduced for intercomparision. In IUM, for urban underlying surfaces, a water balance model was developed using the impervious water depth as the prognostic variable. The Noah Single Layer Urban Canopy Model (Noah/SLUCM) (Chen et al. 2011) and the IUM (Meng 2015) were intercompared using the observed fluxes data at 325-meter Beijing meteorology tower in Beijing. In addition to the comparison of the fluxes in the radiation and energy balance equations, the ISE in waterlogging circumstance was also compared to study the mechanism of urban water balance processes. Through the comparison, the key factors and physical processes in the urban land surface model were found out.

2. Model and Data

2.1 Model

Three main control equations exist in the land surface model; they are radiation balance model, energy balance model and water balance model. We compared all

https://doi.org/10.5194/gmd-2019-298
Preprint. Discussion started: 24 February 2020

the simulated fluxes in the radiation and energy balance equations with the observation. The radiation balance model could be described as follows:

$$R_n = S\downarrow + L\downarrow - S\uparrow - L\uparrow \qquad (1)$$

Where R_n is the net radiation (W m^{-2}); $S\downarrow$ is the downward solar radiation; $L\downarrow$ is the downward longwave radiation (W m^{-2}); $S\uparrow$ is the upward solar radiation (W m^{-2}); $L\uparrow$ is the upward longwave radiation (W m^{-2}).

The energy balance model could be described as follows:

$$R_n = H + LE + G + A \qquad (2)$$

Where H is the sensible heat flux (W m^{-2}); L is the latent heat of evaporation for water (W m^{-2}); E is the evapotranspiration (W m^{-2}); LE is the latent heat flux (W m^{-2}); G is the ground heat flux (W m^{-2}); A is the AHR (W m^{-2}), which used the same diurnal cycle data for the two models.

As this paper focuses on the fluxes in urban areas, only the parameterization schemes of the fluxes in urban areas is given blow. The detailed parameterization scheme of the models could be seen in relevant papers (Chen and Dudhia, 2001; Meng, 2015).

2.1.1 Noah/SLUCM

The Noah Land Surface Model (Noah LSM) (Chen et al. 1996; Chen and Dudhia 2001; Ek et al. 2003) has been implemented in the fifth-generation Pennsylvania State University–NCAR Mesoscale Model (MM5) and the weather research and forecasting (WRF) model. It was developed by National Center for Atmospheric Research (NCAR), National Centers for Environmental Prediction (NCEP), the U.S. Air Force Weather Agency (AFWA), and the university community. The single-layer urban

https://doi.org/10.5194/gmd-2019-298
Preprint. Discussion started: 24 February 2020

canopy model (SLUCM) was developed by Kusaka *et al*. (2001) and Kusaka and Kimura (2004). It assumes infinitely-long street canyons parameterized to represent urban geometry, but recognizes the three-dimensional nature of urban surfaces. The SLUCM has been coupled with the Noah LSM in the community mesoscale WRF Model, version 2.2 (Chen et al. 2011). The fluxes in Noah/SLUCM are divided into three parts; they are fluxes in roof, wall and road respectively.

The upward shortwave radiation is parameterized as follows:

$$S\uparrow = S\downarrow - \left[RS_R + 2H_{GT}S_B + (1-R)S_G\right] \tag{3}$$

Where $S\uparrow$ is the upward shortwave radiation (W m^{-2}); $S\downarrow$ is the downward shortwave radiation (W m^{-2}); R is the normalized roof width; H_{GT} is the normalized building height; S_R, S_B and S_G are the absorbed solar radiation by roof, wall and road respectively (W m^{-2}).

The upward longwave radiation is parameterized as follows:

$$L\uparrow = L\downarrow - \left[RR_R + 2H_{GT}R_B + (1-R)R_G\right] \tag{4}$$

Where $L\uparrow$ is the upward longwave radiation (W m^{-2}); $L\downarrow$ is the downward longwave radiation (W m^{-2}); R_R, R_B and R_G are the absorbed longwave radiation by roof, wall and road respectively (W m^{-2}).

The sensible heat flux is parameterized as follows:

$$H = RH_R + 2H_{GT}H_B + (1-R)H_G \tag{5}$$

Where H is the sensible heat flux (W m^{-2}); H_R, H_B and H_G are the sensible heat flux from roof, wall and road respectively (W m^{-2}).

The ISE is parameterized as follows:

$$E_{imp} = RE_R + 2H_{GT}E_B + (1-R)E_G \tag{6}$$

https://doi.org/10.5194/gmd-2019-298
Preprint. Discussion started: 24 February 2020

Where E_{imp} is the ISE (mm s^{-1}); E_R, E_B and E_G are the evaporation from roof, wall and road respectively (mm s^{-1}), they are calculated as follows:

$$E_R = Ch_r u_a \beta_r (q_{sr} - q_a) \tag{7}$$

$$E_B = Ch_b u_c \beta_b (q_{sb} - q_c) \tag{8}$$

$$E_G = Ch_g u_c \beta_g (q_{sg} - q_c) \tag{9}$$

Where Ch_r, Ch_b and Ch_g are the heat transfer coefficient from roof, wall and road respectively (mm m^{-1}); u_a and u_c are wind speed in the reference height and canopy respectively (m s^{-1}); β_r, β_b and β_g are the evaporation coefficients that are regulated by the availability of moisture for roof, wall and road respectively; they could be calculated as follows (Miao and Chen, 2014):

$$\beta_g = \begin{cases} \begin{cases} 1.0, & Rain \geq 10mm, \\ 0.5, & 0 < Rain < 10mm, \end{cases} & Rain, \\ \beta_{g,0} e^{(-dt/5)}, & No\ rain, \end{cases} \tag{10}$$

$$\beta_r = \beta_b = \beta_g$$

Where $Rain$ is the daily precipitation; $\beta_{g,0}$ is β_g at the previous step; dt is the time step (h).

q_{sr}, q_{sb} and q_{sg} are the saturated specific humidity for roof, wall and road respectively (kg kg^{-1}); q_a and q_c are the specific humidity for reference height and canopy respectively (kg kg^{-1}).

The ground heat flux is parameterized as follows:

$$G = RG_R + 2H_{GT}G_W + (1-R)G_G \tag{11}$$

Where G is the surface heat flux (W m^{-2}); G_R, G_B and G_G are the surface heat flux from roof, wall and road respectively (W m^{-2}).

https://doi.org/10.5194/gmd-2019-298
Preprint. Discussion started: 24 February 2020

2.1.2 IUM

The Integrated Urban land Model (IUM) (Meng 2015) was developed based on the Common Land Model (CoLM) (Dai et al. 2003). IUM integrates the land surface models for urban and natural land surfaces. For urban land surfaces, the energy balance model was improved and the water balance model for impervious surfaces was developed.

The upward shortwave radiation is parameterized as follows (Dai et al. 2003):

$$S\uparrow = S\downarrow \cdot \alpha \tag{12}$$

Where α is the albedo, which is defined as follows (Dai et al., 2003):

$$\alpha = \left(\alpha_{vis,dif} + \alpha_{nir,dif}\right)/2 \tag{13}$$

Where $\alpha_{vis,dif}$ and $\alpha_{nir,dif}$ are the albedo for visible and near infrared diffuse solar radiation respectively, which are set as the same as the albedo of the saturated soil with darkest color in CoLM, they are 0.05 and 0.1 respectively.

The upward longwave radiation is parameterized as follows:

$$L\uparrow = (1 - L\downarrow)\varepsilon + (1 - F_{\text{cov}})\varepsilon\sigma T_g^4 + F_{\text{cov}}\varepsilon\sigma T_l^4 \tag{14}$$

Where ε is the emissivity; σ is the Stefan-Boltzmann constant (W m^{-2} K^{-4}); F_{cov} is the fractional vegetation cover; T_g is the ground surface temperature (K); T_l is the leaf temperature (K).

The sensible heat flux is parameterized as follows:

$$H = \rho_a c_p \frac{\theta_g - \theta_a}{r_{ah}} = \rho_a c_p \frac{T_g - \theta_a}{r_{ah}} \tag{15}$$

Where ρ_a is the air density (Kg m^{-3}); c_p is the specific heat of dry air (J Kg^{-1} K^{-1}); θ_g is the surface potential temperature (K); θ_a is the air potential

https://doi.org/10.5194/gmd-2019-298
Preprint. Discussion started: 24 February 2020

Geoscientific Model Development Discussions

temperature at reference height (K); r_{ah} is the aerodynamic resistance for sensible heat flux between the atmosphere at reference height and the surface (m s^{-1}), which could be calculated as follow:

$$r_{ah} = vu_* / f_h \tag{16}$$

Where v is the von Karman constant; u_* is the friction velocity (m s^{-1}); f_h is the integral of profile function for heat, which is associated with the thermodynamic roughness.

The ISE in the IUM it is parameterized as follows:

$$E_{imp} = \begin{cases} E_p & (W_{i-1} > 0 \; and \; W_i > 0) \\ \min\left(E_p, \max\left(0, \left(P_{rcp} - D_{rain}\right)\right)\right) & (W_{i-1} > 0 \; and \; W_i = 0) \end{cases} \tag{17}$$

Where E_p is the potential evaporation (m s^{-1}), W_{i-1} is the road water depth (mm) in the previous time step, and W_i is the road water depth (mm) in the current time step. The road water depth is controlled by the road water balance equation which will be discussed in the next part of the paper. E_p can be parameterized as follows:

$$E_p = \frac{1000}{\rho_w} \rho_a \frac{q_{sat} - q_m}{r_d} \tag{18}$$

Where ρ_a is the air density (kg m^{-3}); ρ_w is the water density (kg m^{-3}), which is approximately equal to 1000; r_d is the aerodynamic resistance for evaporation (s m^{-1}); q_m is the specific humidity of the air (kg kg^{-1}); and q_{sat} is the saturated specific humidity of the water surface (kg kg^{-1}). If the water depth is not zero, road surfaces are treated as shallow lakes, and the lake model (Henderson-Sellers 1986; Hostetler and Bartlein 1990; Hostetler et al. 1993) in the CoLM is simplified to

https://doi.org/10.5194/gmd-2019-298
Preprint. Discussion started: 24 February 2020

compute the road water temperature. The simplified shallow lake model can be described as follows:

$$\frac{\partial T_w}{\partial t} = \frac{\partial}{\partial W}\left[(\frac{k_w}{c_w} + k_e) \frac{\partial T_w}{\partial W} \right] + \frac{1}{c_w}\frac{d\phi}{dW} \tag{19}$$

Where T_w is the road water temperature (K), k_w is the thermal conductivity of water (W m^{-1} K^{-1}), k_e is the eddy diffusion coefficient (m^2 s^{-1}), c_w is the heat capacity of water (J m^{-3} K^{-1}), and ϕ is the solar radiation heat source term (W m^{-2}).

The ground heat flux is considered as the remainder of the energy balance equation.

2.2 Data

The Chinese Academy of Sciences 325-m-high Meteorology and Environmental Observation Tower data was used to force the models and for comparison. The tower is located in downtown Beijing, the altitude of the foot of the tower is 49m, the longitude and latitude are 116.3708E and 39.9744N respectively. The turbulent heat fluxes including the sensible heat flux and latent heat flux are measured using the eddy covariance (EC) technique at the 47-meter height. The radiation fluxes including the upward and downward shortwave and longwave radiation are measured using the radiometer at the 47-meter height. The net radiation was calculated using equation 1. The ground heat flux was calculated using equation 2; the AHR was not considered. The Gaofen-2 2m resolution LULC data (Figure 1) was used to calculate the area percentage of each LULC categories. Within a 1000m radius of the tower, the surface is 78.3% impervious (buildings, roads, etc) and 21.7% pervious (trees and grass). The simulation time period is from 1st March to 31st October 2015. The temporal resolution of the two models is 30min.

2.3 Model Parameterization and Initialization

Table 1 listed the sources of the initial values of the time-variant variables, forcing variables, and the values of the time-invariant variables for the two models. In order to ensure the objectivity of the intercomparison, identical values were set up for the variables used both in Noah/SLUCM and IUM. For the variables only used in Noah/SLUCM, the values were parameterized using the default look-up table. All other variables referred by the paper in section 2.1 are intermediate variables, which were calculated by the models themselves. The initial values of soil moisture, surface temperature and soil temperature are from the observation of the tower. The LULC categories are from Gaofen-2 data which referred in the last section. The diurnal cycle of the anthropogenic heat is the same for the two models which is used from Miao et al. (2011). The meteorological forcing data is from the observation of the tower. The leaf area index (LAI) and fractional vegetation cover (FVC) are considered as the forcing variables which calculated using an empirical equation (Dai et al. 2003; Wang et al. 2007) as follows:

$$LAI = LAI_{\max}(LULC) + \left(LAI_{\min}\left(LULC\right) - LAI_{\max}\left(LULC\right)\right)\left(1 - \mathrm{f}\right) \tag{20}$$

$$FVC = 1 - \exp\left(-K \cdot LAI\right) \tag{21}$$

Where LAI is the LAI; $LAI_{\max}$ is the maximum LAI; $LAI_{\min}$ is the minimum LAI; $LULC$ is the LULC; f is the coefficient to calculate LAI, which is associated with the soil temperature in a certain soil depth, above this depth, 90 percent root fraction was included; FVC is the FVC; K is the direct solar extinction coefficient, which is associated with the leaf angle distribution factor which is designated according to the LULC.

https://doi.org/10.5194/gmd-2019-298
Preprint. Discussion started: 24 February 2020

Geoscientific Model Development Discussions

3. Results and Discussion

3.1 Radiation Balance

The upward shortwave radiation is determined by the albedo. The albedo is zero at night. From the daily mean (Figure 2a) and diurnal cycle (Figure 2b) of upward shortwave radiation, it is concluded that the simulation result of IUM is very good compared with the observation especially from 9:00 to 16:00. The Albedo in Noah/SLUCM is too large compared with the observation. Albedo is very important in radiation balance, the remote sensing retrieved albedo (Xu and Shu 2014) should be assimilated into land surface model in the future.

The upward longwave radiation (Figure 3) is associated with the emissivity and the surface radiative temperature. The simulated upward longwave radiation is higher than the observation in the daylight. Compared with that of the Noah/SLUCM, the upward longwave radiation simulated by IUM has a greater deviation from 8:00 to 17:00, as the ground surface temperature simulated by IUM is too high during this time period. In IUM, the solar radiation absorption of the ground surface is overestimated as the shading effect of urban canopy and buildings and the multiple scattering of the solar radiation are not considered (Wang et al. 2016). In order to improve the simulation performance of IUM, the reduction coefficient of solar radiation absorption which is associated with the urban canyon direction, building height, road width ratio, sky view factor, and fractional vegetation cover etc. should be considered. For Noah/SLUCM, the simulated upward longwave radiation is a little higher than the observation at night; while for IUM, it is a litter lower than the

https://doi.org/10.5194/gmd-2019-298
Preprint. Discussion started: 24 February 2020

observation. Due to the complicated parameterization of the UCM, the Noah/SLUM is superior to IUM in upward longwave radiation modeling.

Figure 4 shows the simulated net radiation compared with the observation. The net radiation is also an important component in surface energy balance (Offerle et al. 2003). The observed net radiation is calculated by equation 1; it is associated with the upward shortwave and longwave radiation. The net radiation is underestimated by both the two models from 8:00 to 20:00. Compared with that of the Noah/SLUCM, the IUM can simulate the net radiation better both in the daylight and at night. The net radiation is considered as the remainder of the surface radiation balance equation; the simulation results are depended on both the upward shortwave and longwave radiation.

3.2 Energy Balance

The sensible heat flux is associated with the ground surface temperature and the heat transfer resistance. The heat transfer resistance is associated with the thermodynamic roughness and the friction velocity (See eq. 15). For urban land surface, the thermodynamic roughness and friction velocity are relatively larger than those in the natural surface. The parameterization of friction velocity should be studied in the future in order to improve the simulation of sensible heat flux. The simulated sensible heat flux for Noah/SLUCM and IUM are apparently larger than those of the observation in the daylight. Compared with that of the Noah/SLUCM, the sensible heat flux simulated by IUM has a greater deviation, as the ground surface temperature simulated by IUM is too high in the daylight especially from 9:00 to 17:00 (Figure 5). At night, the simulation of IUM is compared well with the observation. Due to the complicated parameterization of the UCM, the Noah/SLUM

https://doi.org/10.5194/gmd-2019-298
Preprint. Discussion started: 24 February 2020

is superior to IUM in sensible heat flux modeling too.

The ISE parameterization schemes for Noah/SLUCM and IUM are different (See eq. 10 and 17). For Noah/SLUCM, it is associated with the precipitation; while for IUM, it is associated with the surface water depth, precipitation and drainage. From figure 6, it is concluded that the simulated ISE by IUM is apparently larger than that simulated by Noah/SLUCM both in the daylight and at night; but it is still lower that of the observation. One of the reasons is the accuracy of the impervious surface percentage is questionable; the other reason is the drainage is hard to parameterize. The characteristic scale of the observed fluxes is crucial important for urban heterogeneous underlying surfaces. Except for these limitations, urban water balance model is still important in the parameterization of ISE; this would be discussed at length in the next section.

Figure 7 is the simulated ground heat fluxes compared with the observation. The ground heat temperature is associated with the ground temperature and the soil temperature in the second layer; it is considered as the remainder term of the surface energy balance equation for observation. Noah/SLUCM has four soil layers; while IUM has 10 layers. The ground heat flux is underestimated by all the two models in the daylight from 8:00 to 18:00. Compared with that of the Noah/SLUCM, the simulated by IUM has a greater deviation during this time period. As the Noah/SLUCM is superior to IUM in the simulation of urban surface temperature, the ground heat flux simulation of Noah/SLUCM is also better than that of IUM compared with the observation. IUM should be coupled with SLUCM to improve the simulation performance in upward longwave radiation, sensible and ground heat flux.

https://doi.org/10.5194/gmd-2019-298
Preprint. Discussion started: 24 February 2020

Geoscientific Model Development Discussions

3.3 Urban Water Balance

The ISE is an important parameter in urban water balance (Yang et al. 2015). The water depth in impervious surface is an important parameter in urban waterlogging study which is not included in the Noah/SLUCM. In IUM, the water depth in impervious surface is considered as the prognostic variable of urban balance equation. The urban water balance equation in IUM could be described as follows:

$$\frac{\partial W}{\partial t} = P_{rcp} - I_{roof} - E_{imp} - D_{rain} - P_{er} I_{nf} \quad (22)$$

Where W is the water depth on impervious surface (mm); I_{roof} is the roof rainfall interception (mm s^{-1}) (Nakayoshi et al, 2009); P_{er} is the percentage of the pervious surface; and I_{nf} is the infiltration rate (mm s^{-1}).

An empirical equation is developed in Noah/SLUCM to parameterize the ISE, it is only associated with the daily precipitation and the time step (Eq. 10). Figure 8 shows the observed precipitation and simulated water depth by IUM during the simulation period (Figure 8). The drying of the impervious surface should last a period of time. As the result, the impervious surface evaporation is not just associated with the daily precipitation. For IUM, the ISE is parameterized based on the physical mechanisms which control the urban water balance and urban water temperature (Eq. 17-19, 22).

Figure 9 is the observed and simulated diurnal cycle of the latent heat fluxes in waterlogging days. Apparently, the simulated ISE of Noah/SLUCM is smaller than that of the observation. ISE plays an important role in rainy days; the simulation of latent heat flux by IUM is increased compared with that of Noah/SLUCM and it is very close to the observation both in the daylight and at night. The urban water balance model

https://doi.org/10.5194/gmd-2019-298
Preprint. Discussion started: 24 February 2020

is indispensable in urban latent heat flux simulation and urban hydrology research.

3.4 Quantitative Comparison

Figure 10 is the scatted plots of the simulated upward shortwave radiation, upward longwave radiation, net radiation, sensible heat flux, latent heat flux and ground heat flux by the simulation of Noah/SLUCM and IUM compared with the observation. Table 2 and figure 11 are the biases, mean errors (MEs), root mean square errors (RMSEs) and correlation coefficients (Rs) of these fluxes simulated by the two models compared with those of the observations. Compared with the Noah/SLUCM, IUM simulated the upward shortwave radiation quite well. The bias, ME and RMSE are 0.32W/m^2, 2.74 W/m^2 and 5.03 W/m^2 respectively. Both two models overestimate the upward longwave radiation and the sensible heat flux; the deviation of IUM is larger than that of Noah/SLUCM. Both models underestimate the net radiation and the latent heat flux; the deviation of IUM is smaller than that of Noah/SLUCM. Both models underestimate the ground heat flux, the deviation of IUM is larger than that of Noah/SLUCM. Through the quantitative comparison, it is concluded that the Noah/SLUCM can simulate the urban surface temperature, sensible heat flux and upward longwave radiation well; while the IUM could simulate the ISE more accurately. The simulation result of the upward shortwave radiation is depended on the albedo.

4. Conclusions

In this paper, the Noah/SLUCM and IUM were intercompared using the observed fluxes data at 325-meter meteorology tower in Beijing. Through the comparison, the key factors and physical processes of the urban land surface model were found out.

https://doi.org/10.5194/gmd-2019-298
Preprint. Discussion started: 24 February 2020

The characteristic scale of the observed fluxes is crucial important for urban heterogeneous underlying surface. The albedo is an important factor in surface radiation partition. In order to improve the simulation accuracy, remote sensing retrieved albedo should be assimilated into land surface model. The solar radiation absorption of urban surface is reduced by the multiple scattering, absorption of building roof and wall, and shading effect of urban canopy and tall buildings. The reduction coefficient of solar radiation absorption is associated with the urban canyon direction, building height, road width ratio, sky view factor, and fractional vegetation cover etc. Urban thermodynamic roughness and friction velocity are important in urban sensible heat flux simulation. Urban thermodynamic roughness is associated with the height of urban canopy. Urban friction velocity is usually larger than that in the rural area. The drying of the impervious surface should last a period of time. So, the impervious surface evaporation is not just associated with the daily precipitation. ISE is important in rainy days. The urban water balance model is indispensable in urban latent heat flux simulation and urban hydrology research.

In the near future, the characteristic scale of the observed fluxes should be studied by using the footprint method (Roth et. al, 2017). The World Urban Database and Access Portal Tools (WUDAPT) (Hammerberg et al. 2018) should be used in IUM to parameterize the reduction coefficient of solar radiation absorption. The MODIS retrieved albedo should be assimilated into IUM. The urban thermodynamic roughness and urban friction velocity should be reparameterized too.

https://doi.org/10.5194/gmd-2019-298
Preprint. Discussion started: 24 February 2020

Code and Data Availability

The supplement of the paper includes the data for the 325m tower and the code of the IUM and the Noah/SLUCM.

Author Contributions

C.M. conceived the study and wrote the initial draft of the paper. J.D. drew some the pictures and dealt with the paper. All authors revised the paper.

Competing interests

The authors declare that they have no competing interests.

Acknowledgements

This work was supported by the National Natural Science Foundation of China under Grant 41875125 and 41705086. We thank Institute of Atmospheric Physics (IAP), CAS for Beijing meteorology tower observation data; National Center for Atmospheric Research (NCAR) for Noah/SLUCM.

https://doi.org/10.5194/gmd-2019-298
Preprint. Discussion started: 24 February 2020

References

Best, M. J., and Grimmond, C. S. B.: Key Conclusions of the First International Urban Land Surface Model Comparison Project, Bull. Amer. Meteor. Soc., 96, 805–819, 2015.

Chen, F., Mitchell, K., Schaake, J., Xue, Y., Pan, H.-L., Koren, V., Duan, Q. Y., Ek, M., and Betts, A.: Modeling of land-surface evaporation by four schemes and comparison with FIFE observations, J. Geophys. Res., 101, 7251-7268, 1996.

Chen, F., and Dudhia, J.: Coupling an advanced land surface–hydrology model with the Penn State–NCAR MM5 modeling system. Part I: Model implementation and sensitivity, Mon. Wea. Rev., 129, 569–585, 2001.

Chen, F., Kusaka, H., Bornstein, R., Chingm J., Grimmond, C. S. B., Grossman-Clarke, S., Loridan, T., Manning, K. W., Martilli, A., Miao, S., Sailor, D., Salamanca, F. P., Taha, H., Tewari, M., Wang, X., Wyszogrodzki, A. A., and Zhang, C.: The integrated WRF/urban modelling system: development, evaluation, and applications to urban environmental problems, Int. J. Climatol., 31, 273–288, 2011.

Ching, J., Brown, M., Burian, S., Chen, F., Cionco, R., Hanna, A., Hultgren, T., McPherson, T., Sailor, D., Taha, H., and Williams, D.: National urban database and access portal tool, Bull. Amer. Meteor. Soc., 90, 1157-1168, 2009.

Committee on urban meteorology: Urban meteorology: forecasting, monitoring, and meeting users' needs. Washington, D.C.: The National Academies Press, 2012.

Dai, Y., Zeng, X., Dickinson, R. E., Baker, I., Bonan, G. B., Bosilovich, M. G., Denning, A. S., Dirmeyer, P. A., Houser, P. R., Niu, G., Oleson, K. W., Schlosser, C. A., and Yang, Z.-L.: The common land model, Bull. Amer. Meteor. Soc., 84, 1013-1023, 2003.

Demuzere, M., Harshan, S., Jarvi, L., Roth, M., Grimmond, C. S. B., Masson, V., Oleson,

https://doi.org/10.5194/gmd-2019-298
Preprint. Discussion started: 24 February 2020

Geoscientific Model Development Discussions

K. W., Velasco, E., and Wouters, H.: Impact of urban canopy models and external parameters on the modelled urban energy balance in a tropical city, Q. J. R. Meteorol. Soc., 143, 1581-1596, 2017.

Ek, M. B., Mitchell, K. E., Lin, Y., Rogers, E., Grunmann, P., Koren, V., Gayno, G., and Tarpley, J. D.: Implementation of Noah land surface model advances in the National Centers for Environmental Prediction operational Mesoscale Eta Model, J. Geophys. Res. 108, 8851, doi:10.1029/2002JD003296, 2003.

Grimmond, C. S. B., Oke, T. R., and Steyn, D. G.: Urban water balance 1. A model for daily totals, Water Resour. Res., 10, 1397-1403, 1986.

Grimmond, C. S. B., Blackett, M., Best, M. J., Barlow, J., Baik, J.-J., Belcher, S. E., Bohnenstengel, S. I., Calmet, I., Chen, F., Dandou, A., Fortuniak, K., Gouvea, M. L., Hamdi, R., Hendry, M., Kawai, T., Kawamoto, Y., Kondo, H., Krayenhoff, E. S., Lee, S.-H., Loridan, T., Martilli, A., Masson, M., Miao, S., Oleson, K., Pigeon, G., Porson, A., Ryu, Y.-H., Salamanca, F., Shashua-Bar, L., Steeneveld, G.-J., Tombrou, M., Voogt, J., Young, D., and Zhang, N.: The international urban energy balance models comparison project: first result from phase 1, J. Appl. Meteorol. Clim., 49, 1268-1292, 2010.

Grimmond, C. S. B., Blackett, M., Best, M. J., Baik, J.-J., Belcher, S. E., Beringer, J., Bohnenstengel, S. I., Calmet, I., Chen, F., Coutts, A., Dandou, A., Fortuniak, K, Gouvea, M. L., Hamdi, R., Hendry, M., Kanda, M., Kawai, T., Kawamoto, Y., Kondo, H., Krayenhoff, E. S., Lee, S.-H., Loridan, T., Martilli, A., Masson, V., Miao, S., Oleson, K., Ooka, R., Pigeon, G., Porson, A., Ryu, Y.-H., Salamanca, F., Steeneveld, G.-J., Tombrou, M., Voogt, J. A., Young, D., and Zhang, N.: Initial results from phase 2 of the international urban energy balance models comparison project, Int. J. Climatol., 31, 244-272, 2011.

Hammerberg, K., Brousse, O., Martilli, A., and Mahdavi, A.: Implications of employing detailed urban canopy parameters for mesoscale climate modelling: a comparison between WUDAPT and GIS databases over Vienna, Austria, Int. J. Climatol. 38(Suppl.1), e1241-e1257, 2018.

He, X., Shen, S., Miao, S., Dou, J., and Zhang, Y.: Quantitative detection of urban climate resources and the establishment of an urban climate map (UCMap) system in Beijing, Build. Environ., 92, 668-678, 2015.

Henderson-Sellers, B.: Calculating the surface energy balance for lake a reservoir modeling: a review, Rev. Geophys., 24, 625-649, 1986.

Henderson-Sellers, A., and Brown, V. B.: Project for Intercomparison of Land Surface Parameterization Schemes (PILPS): First science plan, GEWEX Tech Note, IGPO Publ. Series 5, 53 pp, 1992.

Henderson-Sellers, A., Yang, Z. L., and Dickinson, R. E.: The Project for Intercomparison of Land-Surface Parameterization Schemes, Bull. Amer. Meteor. Soc., 74, 1335–1350, 1993.

Henderson-Sellers, A., Pitman, A. J., Love, P. K., Irannejad, P., and Chen, T. H.: The Project for Intercomparison of Land-Surface Parameterization Schemes (PILPS): Phases 2 and 3, Bull. Amer. Meteor. Soc., 76, 489–503, 1995.

Hostetler, S. W., and Bartlein, P. J.: Simulation of lake evaporation with application to modeling lake level variations of Harney-Malheur Lake, Oregon, Water Resour. Res., 26, 2603-2612, 1990.

Hostetler, S. W., Bates, G. T., and Giorgi, F.: Interactive coupling of a lake thermal model with a regional climate model, J. Geophys. Res., 98(D), 5045-5057, 1993.

https://doi.org/10.5194/gmd-2019-298
Preprint. Discussion started: 24 February 2020

Kalnay, E., and Cai, M.: Impact of urbanization and land-use change on climate, Nature, 423, 528-531, 2003.

Kusaka, H., Kondo, H., Kikegawa, Y., and Kimura, F.: A simple single-layer urban canopy model for atmospheric models: comparison with multi-layer and slab models, Bound.-Layer Meteorol., 101, 329–358, 2001.

Kusaka, H., and Kimura, F.: Coupling a single-layer urban canopy model with a simple atmospheric model: impact on urban heat island simulation for an idealized case, J. Meteorol. Soc. Jpn., 82, 67–80, 2004.

Loridan, T., and Grimmond, C. S. B.: Multi-site evaluation of an urban land-surface model: intra-urban heterogeneity, seasonality and parameter complexity requirements, Q. J. R. Meteorol. Soc., 138, 1094-1113, 2012.

Meng, C.: The integrated urban land model, J. Adv. Model. Earth Syst., 7, 759-773, 2015.

Miao, S. G., Chen, F., Li, Q. C., and Fan, S.: Impacts of urban processes and urbanization on summer precipitation: a case study of heavy rainfall in Beijing on 1 August 2006, J. Appl. Meteorol. Clim., 50, 806-825, 2011.

Miao, S. G., and Chen, F.: Enhanced modeling of latent heat flux from urban surfaces in the Noah/single-layer urban canopy coupled model, Sci. China Earth Sci., 57(10), 2408-2416, 2014.

Mitchell, V., Mein, R., and McMahon, T.: Modelling the urban water cycle, J. Environ. Modell. Softw., 16, 615-629, 2001.

Nakayoshi, M., Moriwaki, R., Kawai, T., and Kanda, M.: Experimental study on rainfall interception over an outdoor urban-scale model, Water Resour. Res., 45, W04415, doi:10.1029/2008WR007069, 2009.

https://doi.org/10.5194/gmd-2019-298
Preprint. Discussion started: 24 February 2020

Geoscientific Model Development
Discussions

Offerle, B., Grimmond, C. S. B., and Oke, T. R.: Parameterization of net all-wave radiation for urban areas, J. Appl. Meteorol., 42, 1157-1173, 2003.

Roth, M., Jansson, C., and Velasco, E.: Multi-year energy balance and carbon dioxide fluxes over a residential neighbourhood in a tropical city, Int. J. Climatol., 37, 2679-2698, 2017.

Sun, Y., Zhang, X., Ren, G., Zwiers, F. W., and Hu, T.: Contribution of urbanization to warming in China, Nat. Clim. Change, 6, 706-709, 2016.

Wang, W., Li, Z., and Su, H.: Comparison of leaf angle distribution function: Effects on extinction coefficient and fraction of sunlit foliage, Agr. Forest Meteorol., 143, 106-122, 2007.

Wang, Z., Bou-Zeid, E., and Smith, J. A.: A coupled energy transport and hydrological model for urban canopies evaluated using a wireless sensor network, Q. J. R. Meteorol. Soc., 139(675), 1643-1657, 2013.

Wang, M., Chang, H. C., Merrick, J. R., and Amati, M.: Assessment of solar radiation reduction from urban forests on buildings along highway corridors in Sydney, Urban For. Urban Gree., 15, 225-235, 2016.

Xu. J., and Shu, H.: Assimilating MODIS-based albedo and snow cover fraction into the Common Land Model to improve snow depth simulation with direct insertion and deterministic ensemble Kalman filter methods, J. Geophys. Res. Atmos., 119, 10,684–10,701, 2014.

Yang, J., Wang, Z., Chen, F., Miao, S., Tewari, M., Voogt, J. A., and Myint, S.: Enhancing hydrologic modelling in the coupled weather research and forecasting-urban modelling system. Bound.-Lay. Meteorol., 155, 87–109, 2015.

https://doi.org/10.5194/gmd-2019-298
Preprint. Discussion started: 24 February 2020

Geoscientific Model Development Discussions
Open Access

Table 1 The sources of the initial values of the time-variant variables, forcing variables, and the values of the time-invariant variables for IUM and Noah/SLUCM.

Variables		IUM	Noah/SLUCM
Time-variant	Soil Moisture	Observation	Observation
	Surface temperature	Observation	Observation
	Soil temperature	Observation	Observation
	LULC categories	Gaofen-2	Gaofen-2
Forcing	Anthropogenic heat	Diurnal cycle	Diurnal cycle
	Meteorological forcing	Observation	Observation
	Leaf area index	Empirical equation	Empirical equation
	Fractional vegetation cover	Empirical equation	Empirical equation
Time-invariant	Emissivity of ground	0.96	0.96
	Emissivity of wall	/	0.96
	Emissivity of roof	/	0.96
	Roof level	/	Look-up table
	Roof width	/	Look-up table
	Heat capacity of roof	/	Look-up table
	Heat capacity of wall	/	Look-up table
	Thermal conductivity of roof	/	Look-up table
	Thermal conductivity of wall	/	Look-up table
	Heat capacity of impervious ground surface	2.025×10^6 J $m^{-3}K^{-1}$	2.025×10^6 J $m^{-3}K^{-1}$
	Thermal conductivity of impervious ground surface	2.9 $Wm^{-1}K^{-1}$	2.9 $Wm^{-1}K^{-1}$
	Albedo of roof	/	Look-up table (0.20)
	Albedo of wall	/	Look-up table (0.20)
	Albedo of ground	0.075	0.075
	Street direction	/	Look-up table
	Street width	/	Look-up table
	Building width	/	Look-up table
	Building height	/	Look-up table
	Number of roof layer	/	4

https://doi.org/10.5194/gmd-2019-298
Preprint. Discussion started: 24 February 2020

Roof layer thickness	/	Look-up table
Number of wall layer	/	4
Wall layer thickness	/	Look-up table
Number of road layer	4	4
Road layer thickness (m)	0.0071, 0.028, 0.062, 0.119	0.0071, 0.028, 0.062, 0.119
Roughness length of roof (m)	/	0.01
Roughness length of wall (m)	/	0.0001
Roughness length of ground (m)	0.01	0.01

https://doi.org/10.5194/gmd-2019-298
Preprint. Discussion started: 24 February 2020

Geoscientific Model Development Discussions
Open Access
EGU

Table 2 Biases, mean errors (MEs), root mean square errors (RMSEs) and correlation coefficients (Rs) of the fluxes simulated by the two models compared with those of the observations.

Variables and Models		Biases(W/m²)	MEs(W/m²)	RMSEs(W/m²)	Rs
S↑	**Noah/SLUCM**	11.98	12.73	22.86	0.988
	IUM	0.32	2.74	5.03	0.988
L↑	**Noah/SLUCM**	26.18	26.59	36.58	0.954
	IUM	37.19	46.98	69.25	0.853
Rn	**Noah/SLUCM**	-52.33	52.41	67.93	0.997
	IUM	-31.62	42.57	62.62	0.988
H	**Noah/SLUCM**	39.20	44.65	62.13	0.824
	IUM	47.39	57.45	97.26	0.800
LE	**Noah/SLUCM**	-33.89	42.82	88.20	0.199
	IUM	-25.78	45.60	88.59	0.205
G	**Noah/SLUCM**	-30.71	64.03	105.89	0.856
	IUM	-80.99	111.37	169.85	0.552

https://doi.org/10.5194/gmd-2019-298
Preprint. Discussion started: 24 February 2020

Geoscientific Model Development Discussions

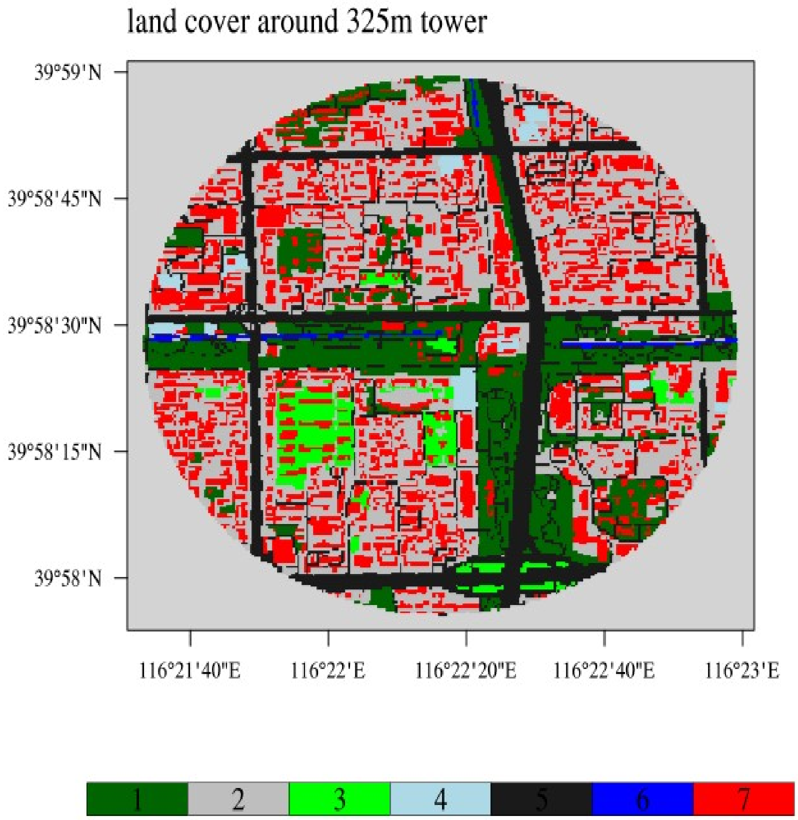

Figure 1 The LULC with 1km radius around the tower from Gaofen-2 2m resolution satellite data

1. Trees; 2. Other impervious surfaces; 3. Grass; 4. Parking lots; 5. Roads; 6. Water; 7. Buildings

https://doi.org/10.5194/gmd-2019-298
Preprint. Discussion started: 24 February 2020

Geoscientific Model Development Discussions

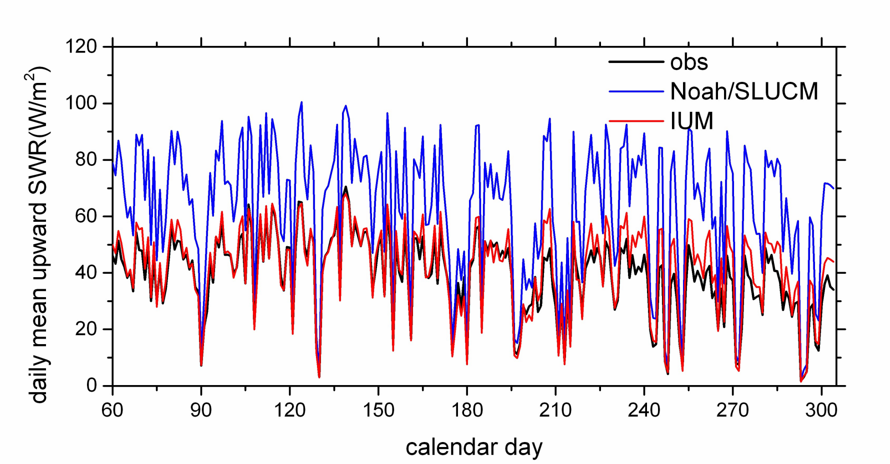

(a)

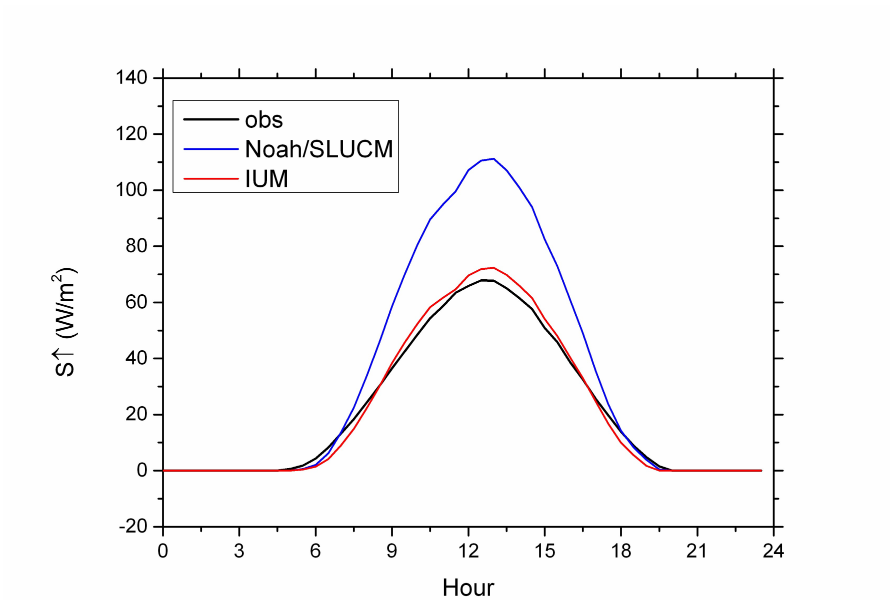

(b)

Figure 2 Daily mean (a) and diurnal cycle (b) upward shortwave radiation simulated by the Noah/SLUCM and IUM compared with the observation.

https://doi.org/10.5194/gmd-2019-298
Preprint. Discussion started: 24 February 2020

Geoscientific Model Development
Discussions
Open Access
EGU

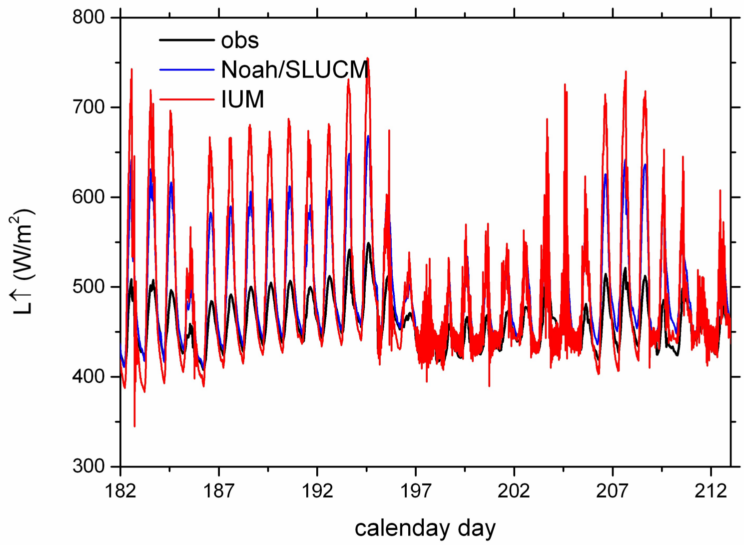

(a)

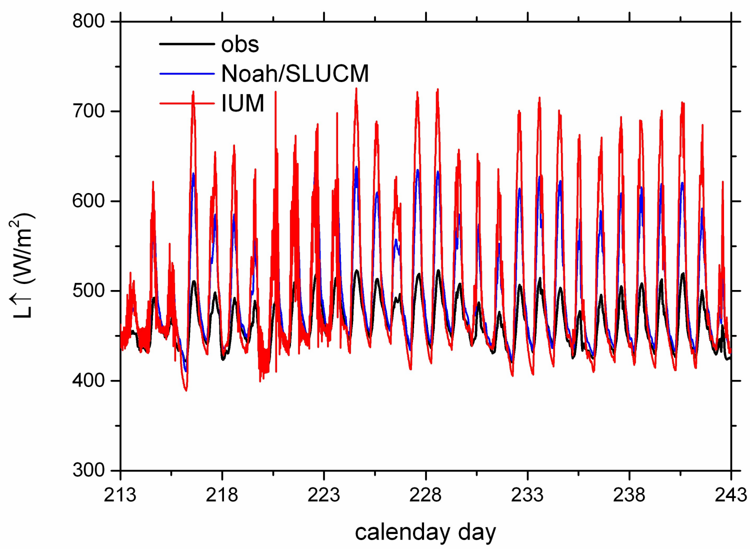

(b)

https://doi.org/10.5194/gmd-2019-298
Preprint. Discussion started: 24 February 2020

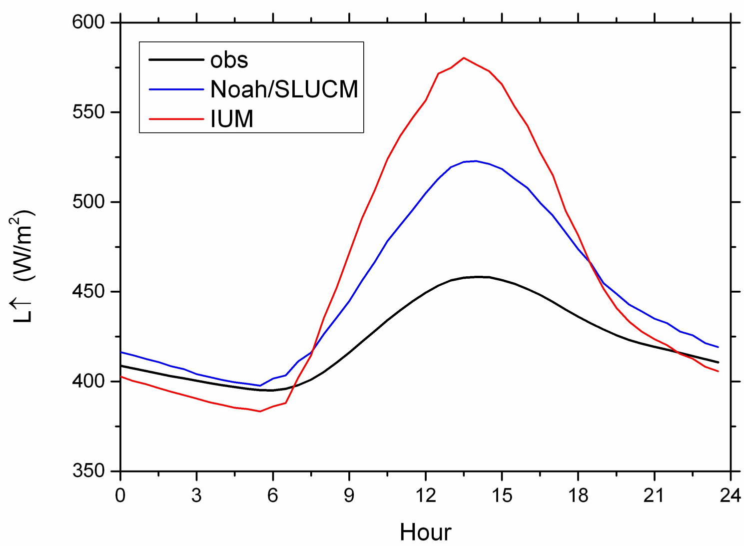

(c)

Figure 3 July (a), August (b) and diurnal cycle (c) upward longwave radiation simulated by the Noah/SLUCM and IUM compared with the observation.

https://doi.org/10.5194/gmd-2019-298
Preprint. Discussion started: 24 February 2020

Geoscientific Model Development
Discussions
Open Access

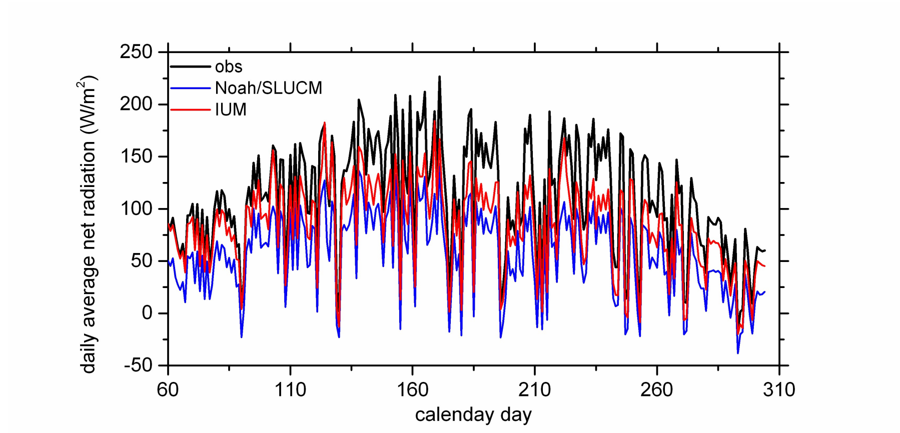

(a)

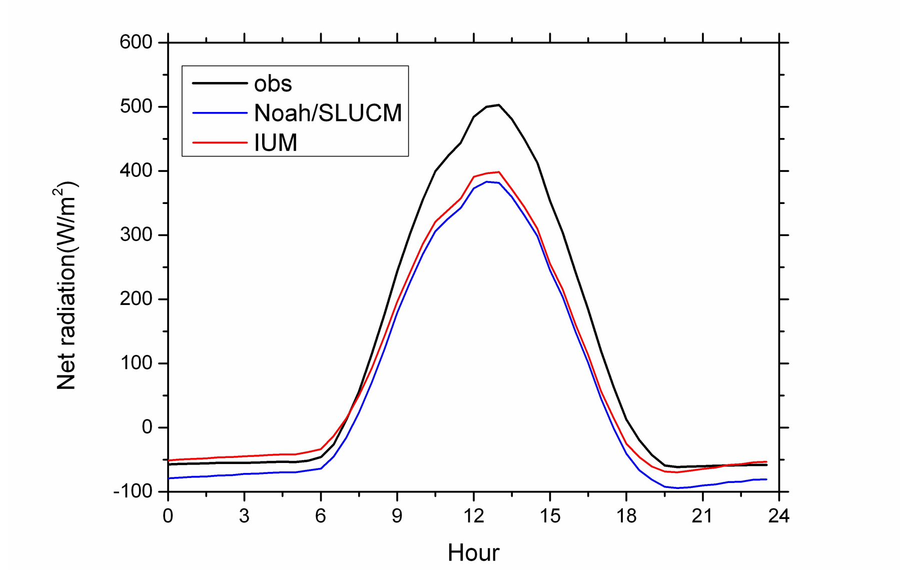

(b)

Figure 4 As figure 2, but for net radiation.

https://doi.org/10.5194/gmd-2019-298
Preprint. Discussion started: 24 February 2020

Geoscientific Model Development Discussions

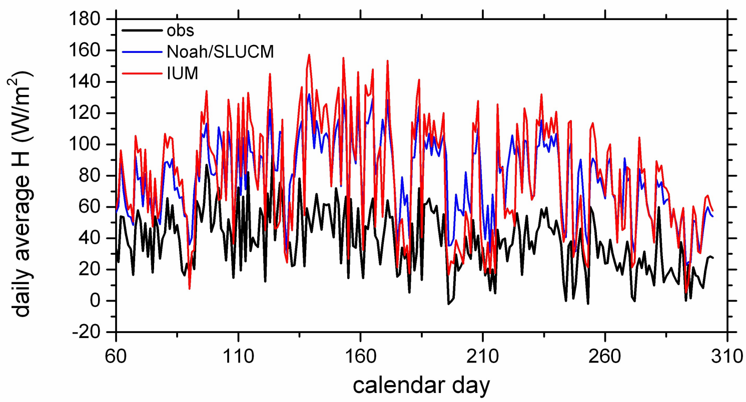

(a)

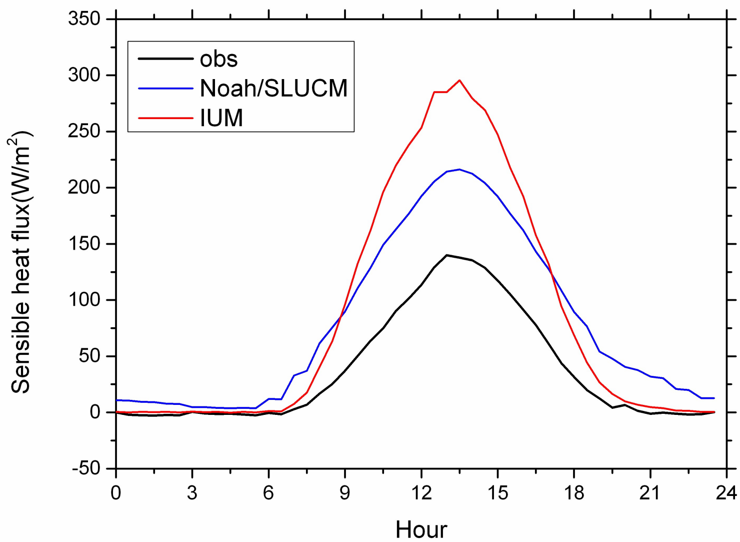

(b)

Figure 5 As figure 2, but for sensible heat flux.

https://doi.org/10.5194/gmd-2019-298
Preprint. Discussion started: 24 February 2020

Geoscientific Model Development
Discussions

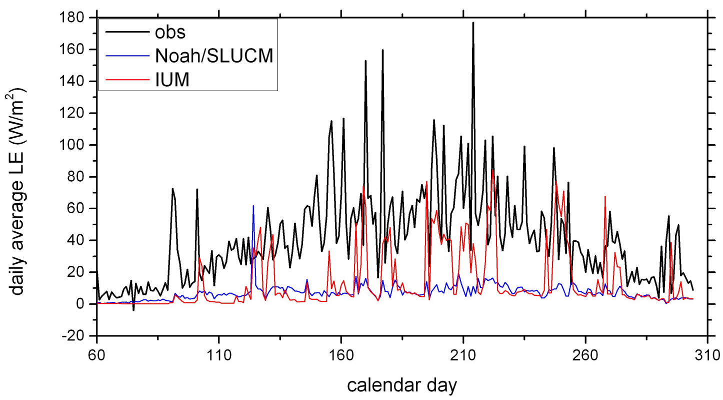

(a)

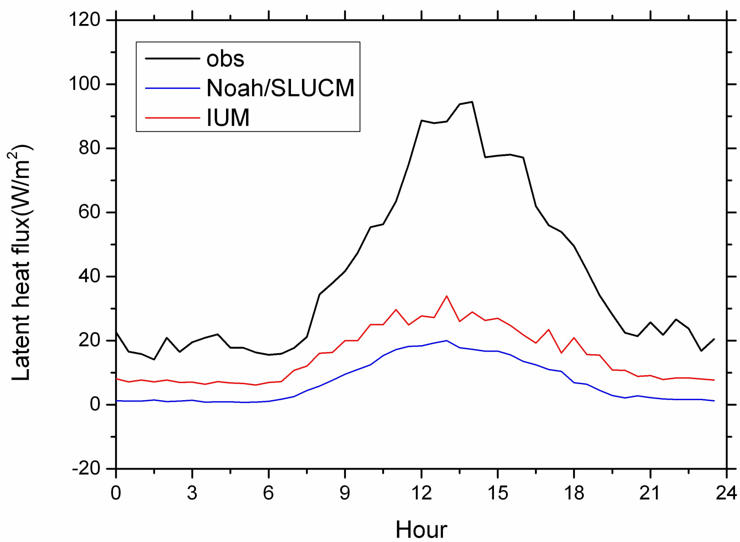

(b)

Figure 6 As figure 2, but for latent heat flux.

https://doi.org/10.5194/gmd-2019-298
Preprint. Discussion started: 24 February 2020

Geoscientific Model Development
Discussions

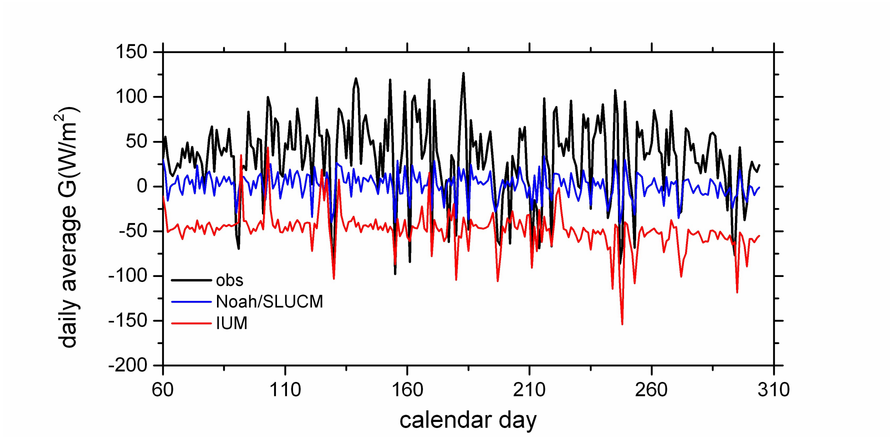

(a)

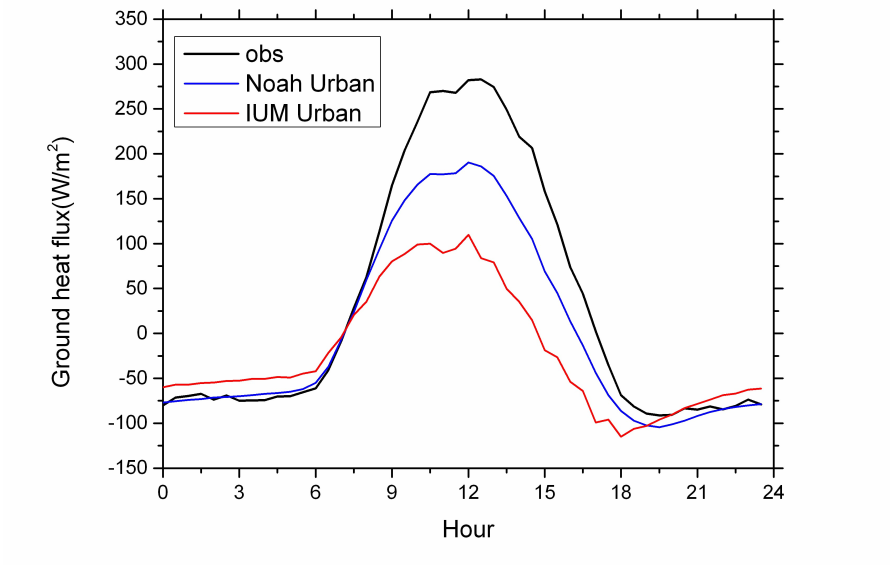

(b)

Figure 7 As figure 2, but for ground heat flux.

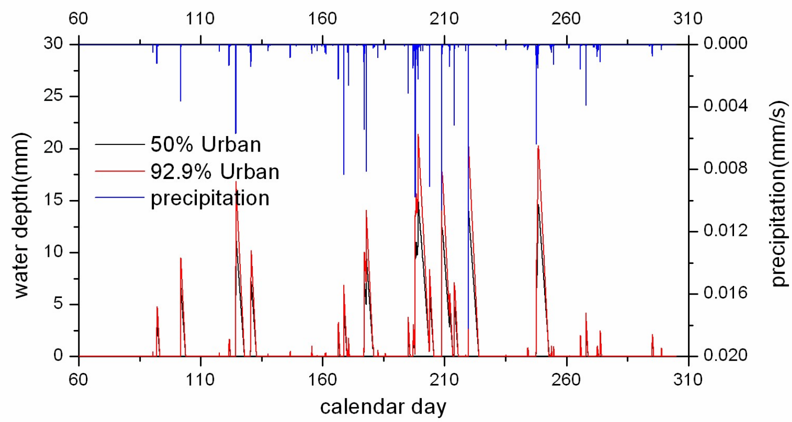

Figure 8 Precipitation and simulated water depth at two circumstances.

https://doi.org/10.5194/gmd-2019-298
Preprint. Discussion started: 24 February 2020

Geoscientific Model Development Discussions
Open Access EGU

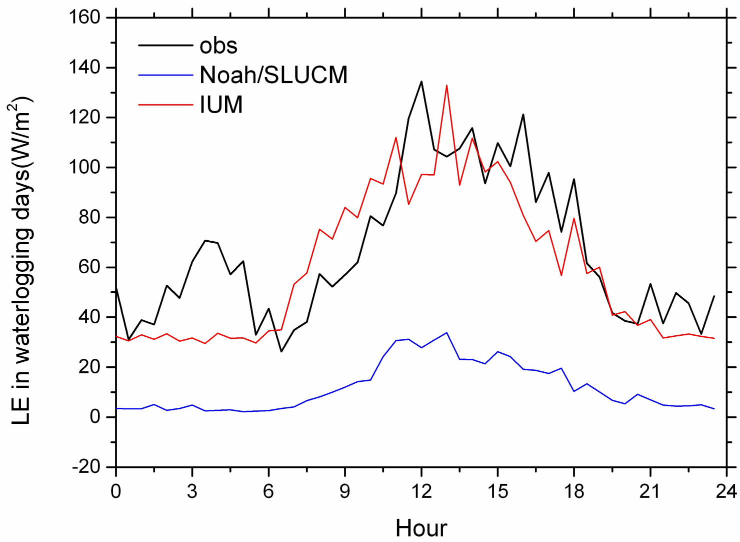

Figure 9 Observed and simulated diurnal cycle of latent heat fluxes in waterlogging days.

https://doi.org/10.5194/gmd-2019-298
Preprint. Discussion started: 24 February 2020

Geoscientific Model Development
Discussions
Open Access

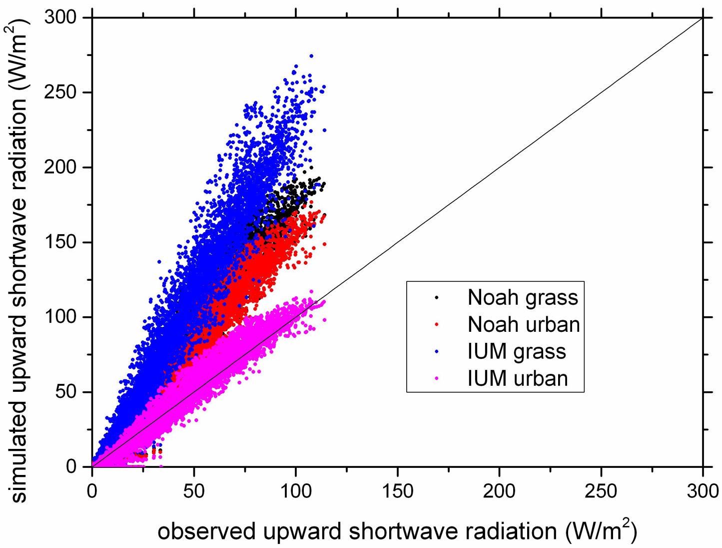

(a)

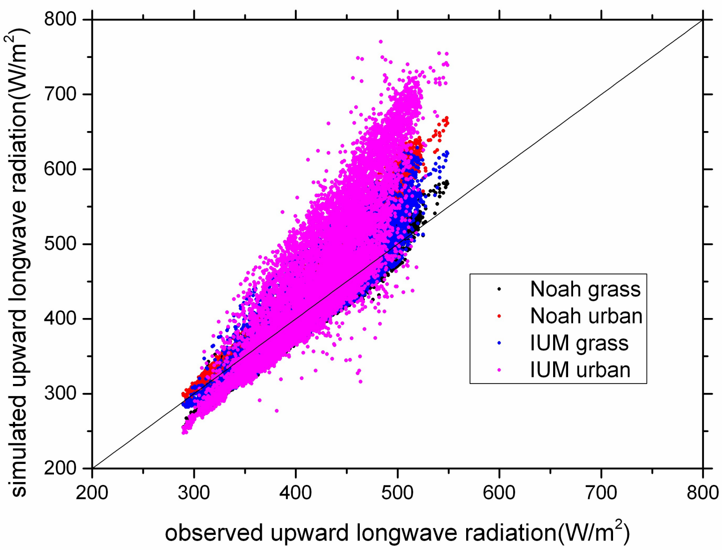

(b)

https://doi.org/10.5194/gmd-2019-298
Preprint. Discussion started: 24 February 2020

Geoscientific Model Development
Open Access
EGU
Discussions

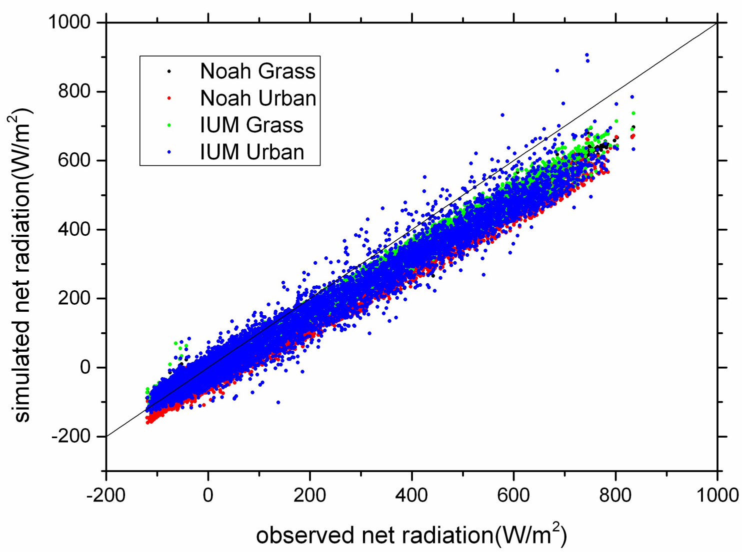

639

640 (c)

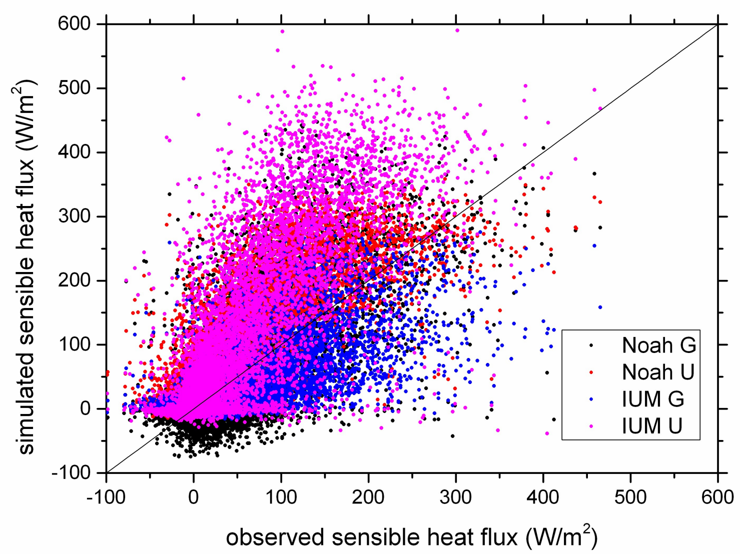

641

642 (d)

https://doi.org/10.5194/gmd-2019-298
Preprint. Discussion started: 24 February 2020

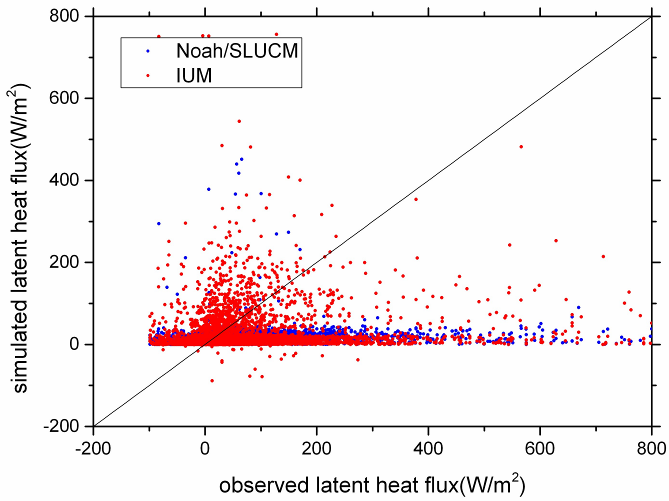

643

644 (e)

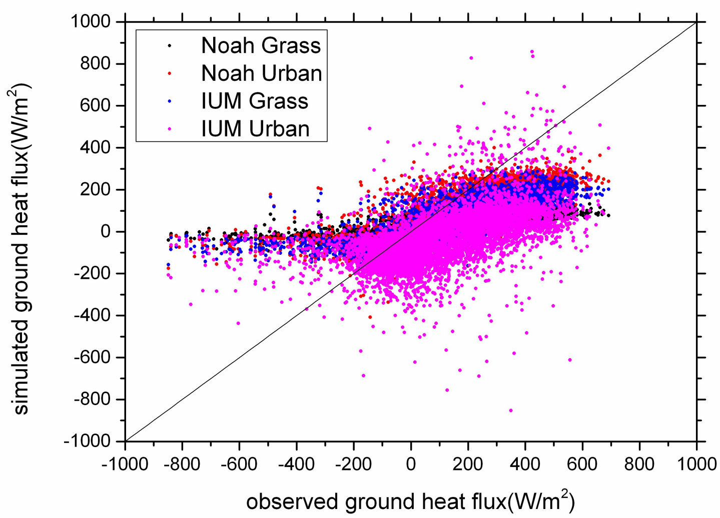

645

646 (f)

647 Figure 10 Scatted plots of the simulated upward shortwave radiation (a), upward longwave

648 radiation (b), net radiation (c), sensible heat flux (d), latent heat flux (e) and ground heat flux

649 (f) compared with the observation.

https://doi.org/10.5194/gmd-2019-298
Preprint. Discussion started: 24 February 2020

Geoscientific Model Development Discussions
Open Access

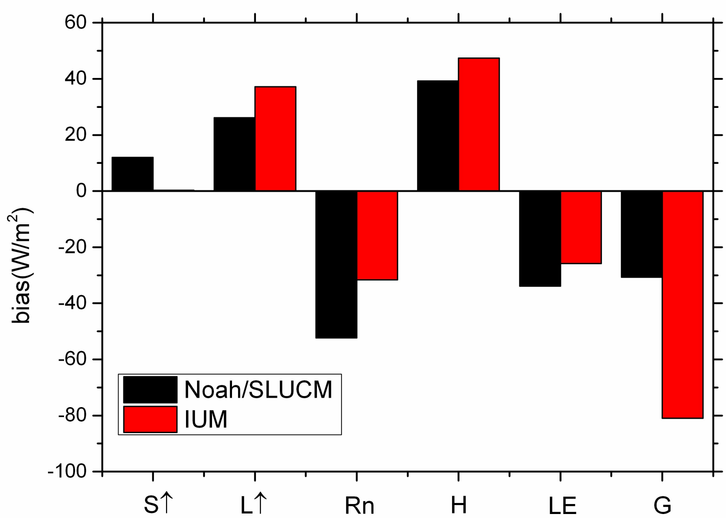

(a)

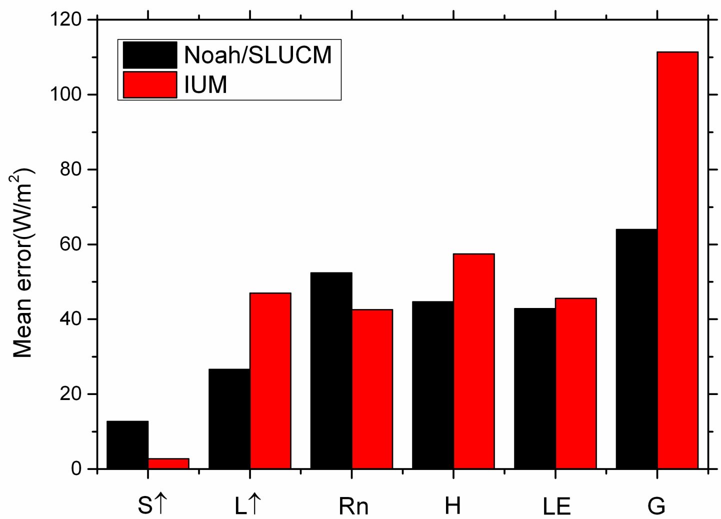

(b)

https://doi.org/10.5194/gmd-2019-298
Preprint. Discussion started: 24 February 2020

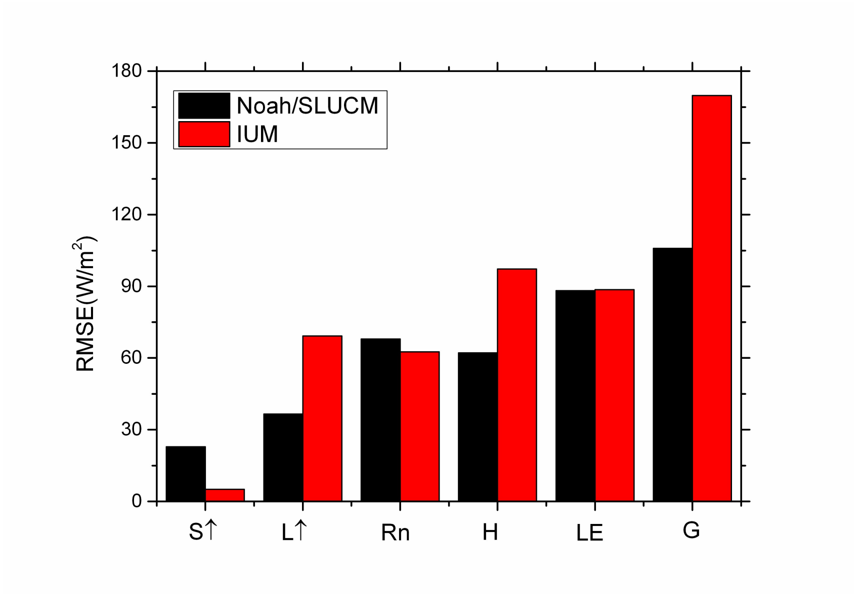

(c)

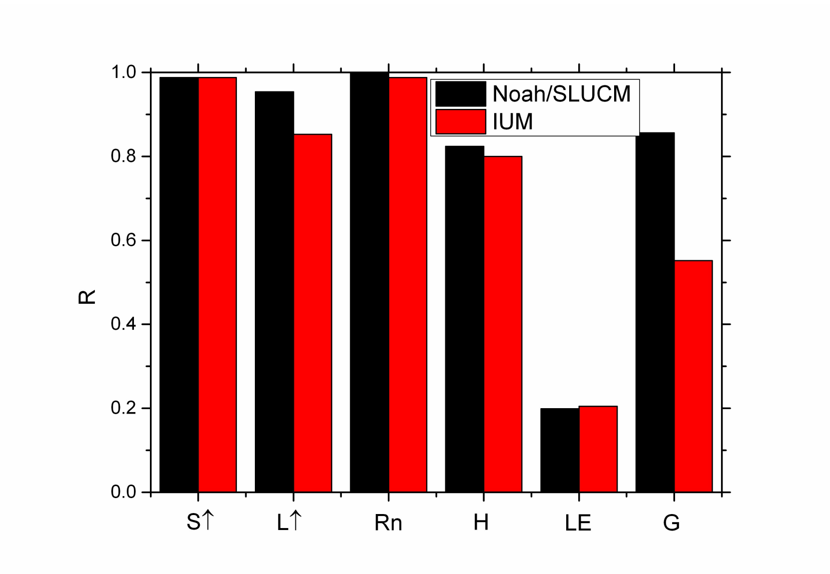

(d)

Figure 11 Biases (a), mean errors (b), root square mean errors (c) and correlation coefficients (d) of the fluxes simulated by the two models compared with those of the observations.